Title

Discovering selective antiferroptotic inhibitors of the 15LOX/PEBP1 complex noninterfering with biosynthesis of lipid mediators

Journal

Proceedings of the National Academy of Sciences of the United States of America, 120(25)

ISSN

0027-8424

Authors

Dar, Haider H
Mikulska-Ruminska, Karolina
Tyurina, Yulia Y
et al.

Publication Date

2023-06-20

DOI

10.1073/pnas.2218896120

PNAS RESEARCH ARTICLE | BIOCHEMISTRY

Discovering selective antiferroptotic inhibitors of the 15LOX/PEBP1 complex noninterfering with biosynthesis of lipid mediators

Haider H. Dar[a,1], Karolina Mikulska-Ruminska[b,1], Yulia Y. Tyurina[a,1], Diane K. Luci[c,1], Adam Yasgar[c], Svetlana N. Samovich[a], Alexander A. Kapralov[a], Austin B. Souryavong[a], Vladimir A. Tyurin[a], Andrew A. Amoscato[a], Michael W. Epperly[d], Galina V. Shurin[a], Melissa Standley[e], Theodore R. Holman[e], Claudette M. St. Croix[f], Simon C. Watkins[f], Andrew P. VanDemark[g], Sandeep Rana[c], Alexey V. Zakharov[c], Anton Simeonov[c], Juan Marugan[c], Rama K. Mallampalli[h], Sally E. Wenzel[a], Joel S. Greenberger[d], Ganesha Rai[c,2], Hülya Bayir[a,i,2], Ivet Bahar[j,2], and Valerian E. Kagan[a,2]

Contributed by Ivet Bahar; received November 25, 2022; accepted May 12, 2023; reviewed by Nikolay V. Dokholyan, Evagelia C. Laiakis, Genevieve Sparagna, and Shinya Toyokuni

Programmed ferroptotic death eliminates cells in all major organs and tissues with imbalanced redox metabolism due to overwhelming iron-catalyzed lipid peroxidation under insufficient control by thiols (Glutathione (GSH)). Ferroptosis has been associated with the pathogenesis of major chronic degenerative diseases and acute injuries of the brain, cardiovascular system, liver, kidneys, and other organs, and its manipulation offers a promising new strategy for anticancer therapy. This explains the high interest in designing new small-molecule–specific inhibitors against ferroptosis. Given the role of 15-lipoxygenase (15LOX) association with phosphatidylethanolamine (PE)-binding protein 1 (PEBP1) in initiating ferroptosis-specific peroxidation of polyunsaturated PE, we propose a strategy of discovering antiferroptotic agents as inhibitors of the 15LOX/PEBP1 catalytic complex rather than 15LOX alone. Here we designed, synthesized, and tested a customized library of 26 compounds using biochemical, molecular, and cell biology models along with redox lipidomic and computational analyses. We selected two lead compounds, FerroLOXIN-1 and 2, which effectively suppressed ferroptosis in vitro and in vivo without affecting the biosynthesis of pro-/anti-inflammatory lipid mediators in vivo. The effectiveness of these lead compounds is not due to radical scavenging or iron-chelation but results from their specific mechanisms of interaction with the 15LOX-2/PEBP1 complex, which either alters the binding pose of the substrate [eicosatetraenoyl-PE (ETE-PE)] in a nonproductive way or blocks the predominant oxygen channel thus preventing the catalysis of ETE-PE peroxidation. Our successful strategy may be adapted to the design of additional chemical libraries to reveal new ferroptosis-targeting therapeutic modalities.

ferroptosis | lipid peroxidation | 15-lipoxygenase | inhibitor design | PEBP1

Significance

Ferroptosis involvement in pathogenesis of several major diseases demands for its new inhibitors. We propose innovative approach for designing inhibitors that act selectively on pro-ferroptotic catalytic complex 15LOX/PEBP1, but not on 15LOX alone. We identified two lead compounds, FerroLOXIN-1 and 2, by structure-activity relationships-guided design, synthesis, and testing of known 15LOX-2 inhibitors, modified to target 15LOX-2/PEBP1 complex. Both FerroLOXINs selectively blocked production of pro-ferroptotic HOO-ETE-PE and protected against RSL3-induced ferroptosis in vitro (in HBE, HT1080, Caco2, A375 and FHs 74 Int. cells) and in vivo (after total body gamma irradiation of mice) without affecting synthesis of essential lipid mediators. Molecular simulations revealed specificity of the mechanism of action of the FerroLOXINs on the 15LOX-2/PEBP1 complex.

Transition to aerobic life and realization of the bioenergetic advantages of the latter required the development of an entirely new and sophisticated system of coordination and regulation of oxygen-driven metabolism and signaling. This relates not only to pathways supporting life but also to the causes and mechanisms of cell death under aerobic conditions (1). Indeed, a number of regulated cell death programs have been discovered and their mechanisms identified (2), whereby an imbalance of redox regulation transitioning into oxidative injury and occurring at different stages of cell's demise, is typical of many, if not all, of these death programs (3). Among them is ferroptosis, for which the disbalance of three major pillars of the redox metabolic platform–iron, thiols, and lipid (per)oxidation–emerged as not an accompanying consequence but rather the initiating mechanism of cell death (4, 5). Research on ferroptosis revealed its likely involvement in the pathogenesis of a variety of acute and chronic disease conditions, including cardiovascular, neurodegenerative, and pulmonary diseases (6–9), cancer (10), asthma (11), brain and kidney injury, and radiation injury (12, 13). Consequently, significant efforts have been deployed toward the discovery of targeted ferroptosis regulators with potential therapeutic effects.

Iron-catalyzed accumulation of phospholipid hydroperoxides and deficiency of the thiol-dependent machinery for their reduction to alcohols has been identified as the primary cause of ferroptotic cell death (14). More detailed studies established that hydroperoxy (HOO)-derivatives of polyunsaturated fatty acid-phosphatidylethanolamines (PUFA-PE), primarily arachidonoyl (AA) (C20:4)- and adrenoyl (C22:4)-acyls, e.g., HOO-AA-PE, are the primary precursors to a multitude of secondary electrophilic cleavage products that form adducts with nucleophilic sites in proteins, penultimately leading to ferroptotic death (15, 16).

[1]H.H.D., K.M.-R., Y.Y.T., and D.K.L. contributed equally to this work.

[2]To whom correspondence may be addressed. Email: ivet.bahar@stonybrook.edu, bantukallug@mail.nih.gov, hb2753@cumc.columbia.edu, or kagan@pitt.edu.

This article contains supporting information online at https://www.pnas.org/lookup/suppl/doi:10.1073/pnas.2218896120/-/DCSupplemental.

Published June 16, 2023.

Two major concepts of either enzymatic or nonenzymatic iron-driven catalysis have been put forward with significant pro- and counterarguments (17). One of the major candidates for generating proferroptotic HOO-AA-PE are nonheme iron (Fe)-containing lipoxygenases, more specifically 15-lipoxygenases (15LOX) (18, 19). Two isoforms, 15LOX-1 and 15LOX-2, expressed in tissue-specific ways, are involved in peroxidative metabolism of all major PUFAs yielding a variety of regulatory lipid mediators (20). Their expression in different tissues is regulated through direct epigenetic modifications or via other stimulators like cytokine (21, 22). The two isoforms are structurally similar (RMSD: 2.1 ± 0.3 Å), while their sequence identity percentage is 37% (23). They both peroxidize PUFA-phospholipids (20), including AA-PE (also called eicosatetraenoyl-PE, ETE-PE). The selectivity and specificity of 15LOX-catalyzed HOO-AA-PE production is conferred on the enzyme via its association with a scaffold protein, PE-binding protein 1 (PEBP1) (11).

The complexation of 15LOX with PEBP1 distinguishes between the broad and physiologically important catalytic function of 15LOX in the biosynthesis of lipid mediators and its highly specific catalytic activity in the 15LOX/PEBP1 complex towards peroxidation of PUFA-PE. This difference opens an opportunity for inhibiting the proferroptotic pathway of PUFA-PE peroxidation by specifically targeting the enzymatic complex, independently of the biosynthesis of lipid mediators by 15LOX. With this in mind, we aimed to discover a new class of antiferroptotic molecules selectively targeting the 15LOX-2/PEBP1 complex rather than 15LOX-2 alone. Here we report on the design, synthesis, screening, and development of such inhibitors suppressing the peroxidative activity of the 15LOX-2/PEBP1 complex. Using a combination of robust computational approaches and a variety of redox lipidomics analyses, we demonstrate the effectiveness of these newly discovered compounds in i) the inhibition of 15LOX-2/PEBP1-induced PUFA-PE peroxidation in biochemical models; ii) the suppression of ferroptosis in cell culture models; and iii) radiomitigative potency related to the suppression of PUFA-PE peroxidation triggered by total body irradiation (TBI). The newly identified inhibitors are proposed as lead compounds for the development of therapeutic interventions to combat the pathogenic effects of ferroptosis.

Results and Discussion

Design and Synthesis of 15LOX-2/PEBP1 Inhibitors. To develop small molecules that can selectively target the 15LOX-2/PEBP1 complex, we used three previously reported 15LOX-2 inhibitors (24, 25) as the starting point (labeled as **1**, **2,** and **3** in Fig. 1*A*). We used model of RSL3 (a GPX4 inhibitor)-induced ferroptosis in human bronchial epithelial cells (HBE) to assess the potency of the compounds. The 15LOX-2 inhibitors **1**, **2**, and **3** were ineffective in preventing RSL3-induced ferroptosis compared to a known inhibitor, ferrostatin-1 (Fer-1) (Fig. 1*B*). Our previous experimental and computational evidence suggests that PEBP1 allosteric interaction with 15LOX-2 enlarges the binding pocket to accommodate the larger *sn2*-ETE-PE substrate (19). Therefore, we hypothesized that the inhibitor may require additional structural features to target the larger binding pocket of 15LOX-2/PEBP1. To test this hypothesis, we used a ligand-growing strategy around compound **2** and probed the structure–activity relationships (SAR) for several analogs. We specifically introduced additional lipophilic groups at the 4th and 5th positions of the imidazole core in compound **2** that can fit into the noncanonical binding site and thus interfere with the formation of the 15LOX-2/PEBP1 complex and/or the ensuing catalysis of *sn2*-ETE-PE oxidation (*SI Appendix*, Fig. S1 *A* and *B*). Many compounds with an additional group at the 4th position of the imidazole core rescued RSL3-induced ferroptotic death of HBE cells at ~5 μM concentrations (Fig. 1*B*).

Based on the observed antiferroptotic activities, and their poor inhibitory effect on 15LOX-2 alone, we selected compounds **8-10** and **18** for further testing in a dose-dependent manner using RSL3- or erastin (an inhibitor of cystine/glutamate antiporter)- triggered ferroptosis in HBE cells (Fig. 1*C* and *SI Appendix*, Fig. S2*A*). Our LC-MS analysis confirmed the efficiency of compound **10** in inhibiting RSL3-induced accumulation of proferroptotic molecule, *sn-1*-stearoyl-*sn-2*-hydroperoxy-ETE-PE (15-HpETE-PE) (Fig. 1*D*). These data suggested that the placement of additional groups at the 4th position of the imidazole ring in compound **2** could ensure successful occupation of the enlarged binding pocket in 15LOX-2/PEBP1 and simultaneously reduce the potency against 15LOX-2 alone. Our SAR study further indicated that analogs with more lipophilic groups on the phenyl rings had relatively higher potency probably by mimicking the natural lipid substrate (for example analogs **20**-**24**). The sulfur atom of these compounds (e.g., analog **10**) occupied a site in the proximity of the 15LOX-2 active site iron as reported in the cocrystal structure of compound **1** (25) with 15LOX-2. We hypothesized that replacing the S atom with "NH" could enable deprotonation of the "NH" under physiological pH to generate a nitrogen anion, which could then coordinate the iron at the 15LOX-2 active site. We have therefore synthesized new compounds, labeled as **20**-**24**, upon substituting the S atom in compound **10** by "NH" (Fig. 1*E* and *SI Appendix*, Fig. S2*B*). This replacement indeed provided a significant bump in potency when tested at a single concentration or in dose-dependent experiments (Fig. 1 *B* and *F*). Notably, our SAR study further indicated that electron-withdrawing lipophilic groups either at the *para* position or a disubstitution at the *meta* and *para* positions of the benzyl group provided optimal potency as exemplified by analogs **20**-**23**. Both the "F" and "CF_3" groups on the phenyl rings improved the overall lipophilicity of the molecule required to mimic the natural lipid substrate.

The optimization and the progression of the discovery of 15LOX-2/PEBP1 inhibitors are summarized in Fig. 1*A*. Enzymatic activity of 15LOX-2 measured using a standard substrate, arachidonic acid (AA), established that the compounds tested (**4**-**8**, **10**, **11**, **18**, and **20**-**24**) did not show any significant activity at ≥20 μM. Encouraged by these results, we further investigated the ability of compounds **20**-**24** (Fig. 1*G*) to inhibit RSL3-induced ferroptosis at lower (nanomolar) concentrations. All five compounds exhibited improved antiferroptotic potency (lower half-maximal inhibitory concentrations) (Fig. 1*G*) compared to the first-generation compounds **8-10** and **18** (Fig. 1*C*).

Compounds 20-24 Specifically Inhibit 15LOX-2/PEBP1-Catalyzed Oxidation of *sn-1*-Stearoyl-*sn-2*-Arachidonoyl-PE. We further asked whether these five compounds were specific to the suppression of ETE-PE oxidation by the 15LOX-2/PEBP1 complex vs. 15LOX-2. We utilized a biochemical model where the inhibitory activity was examined using recombinant 15LOX-2±PEBP1 proteins. We performed LC-MS analysis of the products generated from ETE-PE/DOPC liposomes (Fig. 2*A*). As expected, PEBP1 markedly (~twofold) enhanced the oxidation of *sn-1-stearoyl-sn-2*-ETE-PE by 15LOX-2 (Fig. 2*A*). Importantly, neither of the tested five compounds affected the formation of 15-HpETE-PE by 15LOX-2 alone (Fig. 2*B*). In contrast, four of them demonstrated significant inhibition of 15-HpETE-PE production by 15LOX-2/PEBP1 complex (Fig. 2*C*). From these results, we chose compounds **21** and **23** for further evaluation as

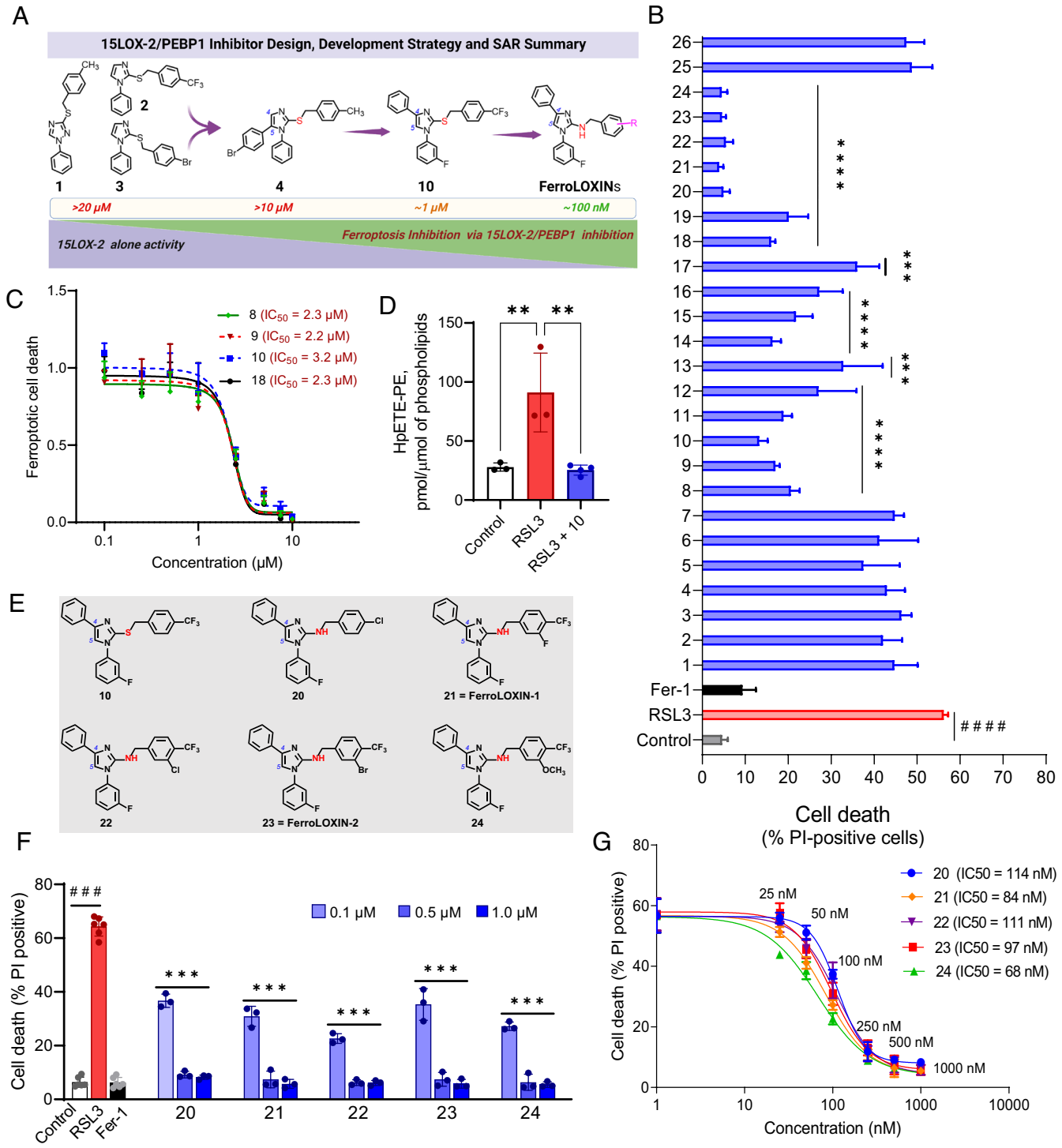

Fig. 1. Development of 15LOX-2/PEBP1 complex specific inhibitors of ferroptosis. (*A*) SAR-guided design of 15LOX-2/PEBP1-specific inhibitors of ferroptosis starting from 15LOX-2 inhibitors (compounds **1**, **2**, and **3**). (*B*) HBE cells were treated with RSL3 (0.5 μM) in the presence of 5 μM compounds 1 to 26. Cell death was estimated after 20 h incubation by PI staining using flow cytometry. Fer-1 (0.2 μM) was used as positive control. $^{\#\#\#}P < 0.0001$ vs. control; $^{***}P < 0.001$ vs RSL3, $^{****}P < 0.0001$ vs. RSL3. One-way ANOVA. (*C*) IC_{50} values of selected compounds **8** to **10** and **18**. HBE cells were treated with RSL3 (0.5 μM) and different concentrations of the compounds. Cell death was estimated relative to that induced by RSL3. (*D*) RSL3-induced accumulation of PE-AA-OOH in HBE cells is inhibited by compound **10**, n = 3, $^{**}P < 0.01$, One-way ANOVA. (*E*) SAR-guided design of compounds **20** to **24** starting from compound **10**. (*F*) HBE cells were treated with RSL3 (0.5 μM) in the presence of different concentration (0.1, 0.5, and 1 μM) of compounds **20** to **24**. n = 3 to 6, $^{\#\#\#}P < 0.001$ vs. control; $^{***}P < 0.001$ vs. RSL3, One-way ANOVA. (*G*) IC_{50} values of selected compounds. HBE cells were treated with RSL3 (0.5 μM) along with different concentrations from 10 to 1,000 nM of compounds **20** to **24.** Data represents mean ± SD, n = 3 or more.

bonafide ferroptotic inhibitors and named them as FerroLOXIN-1 and FerroLOXIN-2, respectively. The structures of FerroLOXIN-1 and FerroLOXIN-2 were confirmed by MS^2 analysis. The presence of a major fragment with m/z 253.1009 was detected in MS^2 spectra of both FerroLOXINs (*SI Appendix*, Fig. S3).

To examine the specificity of FerroLOXINs, we assessed their effects on: i) the generation of proferroptotic 15-HpETE-PE in HBE cells; ii) several alternative cell death programs and iii) RSL3-induced ferroptosis in different cell lines. Redox lipidomics analysis showed that both inhibitors completely prevented the

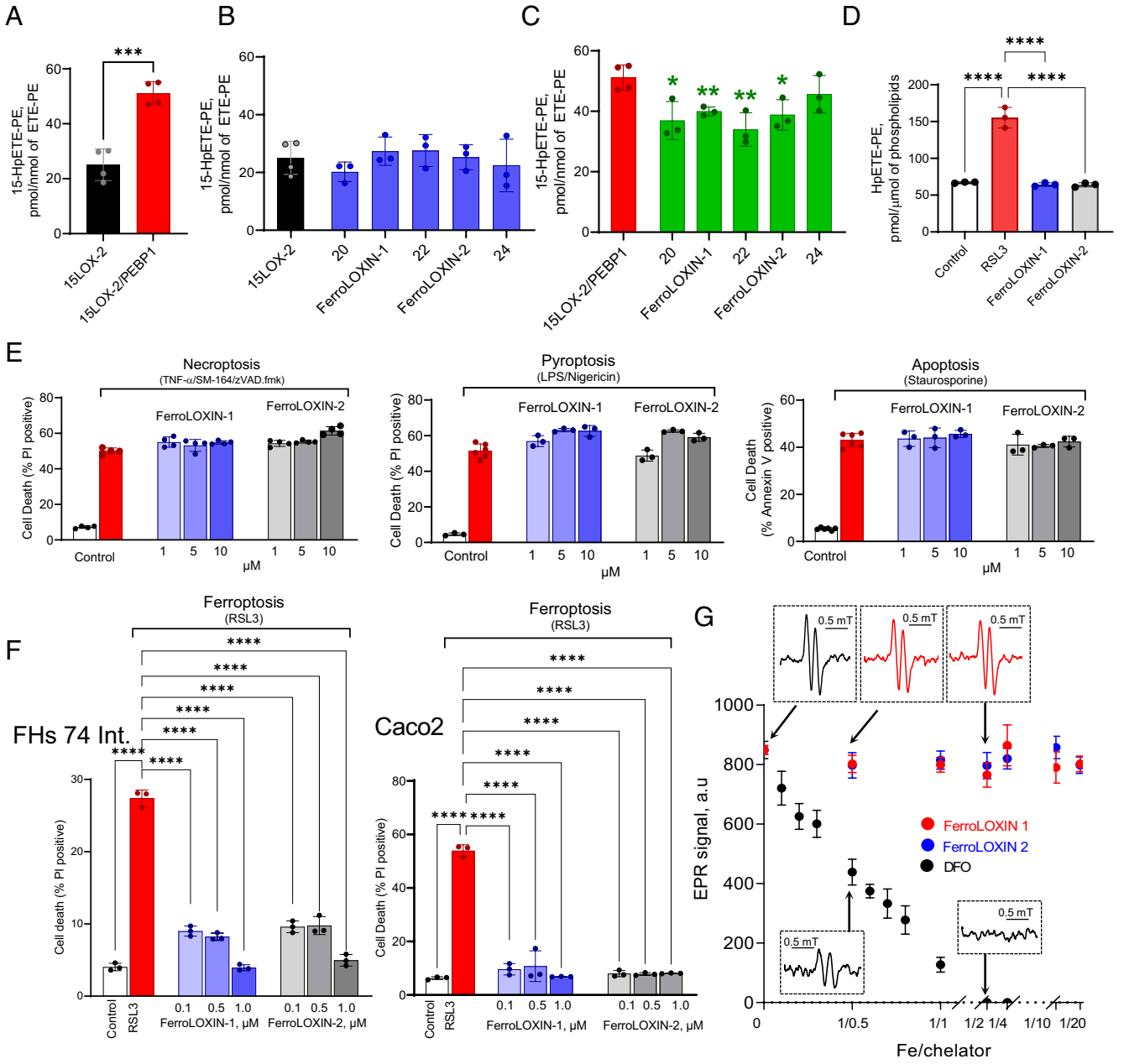

Fig. 2. FerroLOXIN-1 and FerroLOXIN-2 as anti-ferroptotic inhibitors targeting 15LOX-2/PEBP1. (*A*) PEBP1 increases the 15LOX-2 catalyzed oxidation of ETE-PE, n = 4, ***$P < 0.001$, *t* test. Effect of compounds **20**-**24** on the oxidation of ETE-PE by 15LOX-2 alone (*B*) and by the 15LOX-2/PEBP1 complex (*C*), n = 3, *$P < 0.05$, **$P < 0.01$ vs. 15LOX-2/PEBP1, *t* test. (*D*) RSL3-induced accumulation of PE-AA-OOH is inhibited by FerroLOXINs in HBE cells, n = 3, ****$P < 0.0001$, One-way ANOVA. (*E*) FerroLOXINs do not inhibit necroptosis (*Left*) pyroptosis (*Middle*) and apoptosis (*Right*) induced in HBE cells. Necroptosis (TNF-α (20 ng/mL), SM-164 (20 nM), and zVAD.fmk (20 μM) for 18 h), pyroptosis [LPS (1 μg/mL) for 4 and then Nigericin (20 μM) for 2 h] or apoptosis [staurosporine (500 nM) for 2 h] was induced in HBE cells in the absence or presence of FerroLOXINs, n = 3. Cell death was estimated by PI staining (necroptosis/pyroptosis) or Annexin + PI staining (apoptosis). (*F*) FerroLOXINs inhibit ferroptosis in intestinal epithelial cells. FHs 74 Int. or Caco2 cells were treated with RSL3 (0.25 μM or 2 μM) to induce ferroptosis in presence of FerroLOXINs (0.1, 0.5 and 1 μM) for 20 h and cell death was estimated by PI staining. n = 3, ****$P < 0.0001$, One-way ANOVA. (*G*) Magnitudes of the semidehydroascorbyl radical EPR signals formed during the reduction of Fe (III) by ascorbic acid in the presence or absence of FerroLOXINs or DFO. *Inserts:* Typical semidehydroascorbyl radical EPR signal generated during the reduction of Fe (III) by ascorbic acid in the absence (*Upper* panel, black) or in presence of FerroLOXIN-1 (red) or DFO (*Lower* panel, black) at Fe/chelator ratios 1/0.5 and 1/2, respectively. n = 6. Data represents mean ± SD (n = 3 to 6).

formation of proferroptotic 15-HpETE-PE in RSL3-treated HBE cells (Fig. 2*D*). Next, we tested the effects FerroLOXINs on necroptosis, pyroptosis, and apoptosis in HBE cells. Both compounds had no impact even at concentrations 10 times higher than those exerting complete protection against ferroptosis (Fig. 2*E*). Finally, we demonstrated that both FerroLOXIN-1 and 2 fully protected against RSL3-induced ferroptosis in several cell lines: intestinal epithelial cells (Caco2, FHs 74 Int.) and cancer cells (HT-1080, A375) (Fig. 2*F* and *SI Appendix*, Fig. S4).

Antiferroptotic Function of FerroLOXINs Is Independent of Iron Chelation and Radical-Scavenging Activity. The current repertoire of ferroptosis inhibitors includes two major categories: iron chelators forming redox inactive complexes, like deferoxamine (DFO), and radical scavengers, e.g., α-tocopherol. Redox-cycling activity of Fe can be fed by endogenous one-electron reductants, like ascorbate. The intermediate of ascorbate oxidation, ascorbyl radical, can be directly detected by electron paramagnetic resonance (EPR) spectroscopy (26). We used this technique to assess the

ability of FerroLOXINs to quench the Fe-driven oxidation of ascorbate to its radical. Based on the effects on the EPR signals of ascorbyl radicals, we established that the FerroLOXINs did not exert the Fe-chelating activity associated with the quenching of the redox-cycling activity of Fe even at 20:1 (FerroLOXINs:iron) stoichiometry (Fig. 2*G*). In contrast, DFO at 2:1 ratio completely inhibited the Fe-induced ascorbyl radical EPR signal (Fig. 2*G*).

We next assessed the radical-scavenging activity of FerroLOXINs by their interactions with a 2,2-diphenyl-1-picrylhydrazyl (DPPH) radical (27). Both FerroLOXIN-1 and 2 displayed a negligibly low activities toward interaction with DPPH (*SI Appendix*, Fig. S5) (the rates were $>10^3$ lower than that of α-tocopherol). Thus, the mechanism of the effects of the FerroLOXINs on 15LOX-2/PEBP1 and ferroptosis cannot be explained by radical scavenging.

FerroLOXINs Selectively Bind High-Affinity Sites Harbored by 15LOX-2/PEBP1 Complex, Not Observed in 15LOX-2 Alone. To gain insights into the molecular mechanisms of the selective potency of the new inhibitors against 15LOX-2/PEBP1 as opposed to 15LOX-2 alone, we performed a series of docking and molecular dynamics (MD) simulations and principal component analysis (PCA) of the conformational space, as schematically described in *SI Appendix*, Fig. S6. Docking simulations were performed for compounds **21** (FerroLOXIN-1)**, 23** (FerroLOXIN-2), and **24** using four targets: 15LOX-2, 15-LOX-2/ETE-PE, 15LOX-2/PEBP1, and 15LOX-2/PEBP1/ETE-PE. Each target was represented by 3 to 5 conformations deduced using *ProDy* (28) interface from the PCA of MD trajectories (29–31), summing up to a total of 18 target conformational states, each subjected to five independent runs, for each compound. The ribbon diagrams in Fig. 3 and *SI Appendix*, Fig. S7 display the superposition of compound-bound forms from multiple runs. The compounds are in *sticks*, colored from *white* (weak affinity) to *red* (high affinity). They cluster in high-affinity sites, four of which are distinguished as being accessible in 15LOX-2/PEBP1 (bound or unbound to ETE-PE), but not 15LOX-2 alone. These are enclosed in *red* (*Site 1*), *black* (partially overlapping *Sites 2* and *4*) and *purple* (*Site 3*, visible upon 180º rotation of the structure; Fig. 3*B*) *ellipses*. Most probable binding poses to those sites are illustrated in Fig. 3 *C*–*F*.

Before proceeding to the analysis of binding poses and mechanisms, we note that the production of 15-HpETE-PE necessitates the localization of *sn-2* (AA-) chain of ETE-PE within the catalytic site of 15LOX-2, which also harbors the iron ion coordinated by three catalytic histidines and a C-terminal isoleucine (32). In contrast to the *sn-1* (S, stearoyl) chain, the *sn-2* AA-chain contains *bis*-allylic moieties, and 15LOX-2 catalyzes the insertion of an oxygen to the carbon atom C15 of the *sn-2* chain (33). As will be shown below, the binding poses include one (*Site 3*) that obstructs the O_2 channel crucial to the peroxidation (Fig. 3 *B* and *E*), and another (*Site 4*) that disrupts the precise positioning of ETE-PE *sn-2* chain and places instead the *sn-1* chain at the catalytic pocket (*Site 4*, panel *F*).

Sites 1 and 2 (Fig. 3 *C* and *D*) were both located at the 15LOX-2/PEBP1 binding interface with the *sn-2* (AA) chain of ETE-PE bound to the catalytic pocket. The compounds in *Site 1* were consistently coordinated by 15LOX-2 F184, G186 and L609 (at first or second coordination shells around the catalytic pocket) and PEBP1 W84, D144 and H145. Those in *Site 2* were coordinated by PEBP1 R141-D144, R146 and 15LOX-2 Q187 and S190 (Fig. 3*D*). *Site 3* was at the entrance of the frequently accessed O_2 channel, and FerroLOXIN-1 and 2 closely interacted therein with 15LOX-2 only, and in particular with Y154, N155, W158 (Fig. 3*E* and *SI Appendix*, Fig. S8 *C* and *D*). These residues were reported in previous studies to locate at the O_2 channeling gate (29, 30). Interestingly, compound **24** did not bind to *Site 3*, presumably due to its bulky methoxy group (*SI Appendix*, Fig. S8*B*). Binding of compounds to *Site 4*, on the other hand, promoted the insertion of the *sn-1* tail of ETE-PE into the catalytic site. Thus, in this case, nonproductive interaction between the complex and the nonoxidizable stearoyl chain appears to be the mechanism of suppression of ETE-PE peroxidation (Fig. 3*F*). Binding energies of compounds to *Sites 1-2* and *4* were comparable, and those to *Site 3* were slightly weaker (*SI Appendix*, Table S1).

Overall, these computations show that the 15LOX-2/PEBP1 harbors high-affinity sites presented by the complex only, and not by the unbound 15LOX-2, for binding the newly discovered compounds. *Sites 1, 2,* and *4* are localized at the interface between PEBP1 and 15LOX-2 and may allosterically affect the catalytic function of 15LOX-2, whereas *Site 3* may block the diffusion of oxygen atoms to the catalytic pocket. Simulations presented next further clarify their inhibitory mechanisms and specificities.

FerroLOXINs Act by Blocking O_2 Entry, and/or Dislodging the Oxidizable *sn*-2 (AA) Chain from, or Stabilizing the Nonoxidizable *sn*-1 Chain at, 15LOX-2 Catalytic Pocket. We performed MD simulations (a total of 7.4 μs; see *SI Appendix*, Table S2) to gain a molecular understanding of the specific interactions of the target protein/complex and compounds, FerroLOXIN-1 and 2, and **24**. *SI Appendix*, Table S3 lists the 15LOX-2 and PEBP1 residues that exhibited persistent interactions with these inhibitors.

Site 1 was the highest affinity site (*SI Appendix*, Table S1). All three compounds remained stably bound to this site in multiple runs. Both FerroLOXINs dislodged the "buried" oxidizable *sn-2* acyl chain from the catalytic site, either partially or completely (Movie S1 and *SI Appendix*, Fig. S9*B*). Simultaneously, they weakened the *sn-1* ETE-PE/PEBP1 contacts as well as those between 15LOX-2 and PEBP1, upon insertion into the interfacial regions between 15LOX-2 and its substrates. Compound **24** adopted a slightly different conformation than the other two, due to its methoxy group ($O\text{-}CH_3$) instead of bromine (F) or fluorine (Br) in FerroLOXIN-1 and 2, respectively, and its propensity to dislodge the *sn-2* chain was relatively lower.

FerroLOXIN-2 binding to *Site 2* caused a displacement of the oxidizable *sn-2* chain partially out of the catalytic site. In contrast, compound **24** did not induce such a dislocation, thus allowing for the peroxidation to proceed. Binding of either **24** or FerroLOXIN-2 to *Site 4*, on the other hand, stabilized the ETE-PE with a nonoxidizable chain in the proximity of the catalytic iron, thus slowing down the production of 15-HpETE-PE. Both compounds exhibited strong associations with P192-I197 (15LOX-2) and E83, R129, L131, G147, K148, V151, A152, R155 and K156 (PEBP1) (*SI Appendix*, Table S3). Finally, in the case of *Site 3*, both FerroLOXIN-1 and FerroLOXIN-2, but not **24,** blocked an oxygen channel entry as can be seen in Movies S2 and S3. *SI Appendix*, Fig. S10 shows the time evolution of contacts between the FerroLOXINs and 15LOX-2 residues Y154, N155, L419, P423-Q425, G437-F438, and L441, distinguished by their role in stabilizing the compounds at this site.

FerroLOXIN-1 and 2 Rescued Mice from Total Body Radiation-Induced Death by Inhibiting Ferroptosis. To assess the efficacy of FerroLOXIN-1 and 2 in vivo, we evaluated the pharmacokinetic (PK) profiles of both compounds in the plasma and intestine of mice following an intraperitoneal injection (IP) of 25 mg/kg dose. We found that both compounds displayed excellent PK profiles with compound exposure levels much higher than the cellular IC_{50s} and desirable terminal long half-life of 12.1 and 7.5 h with lower clearance (Cl) rates of 17.7 and 12.5 mL/min/kg,

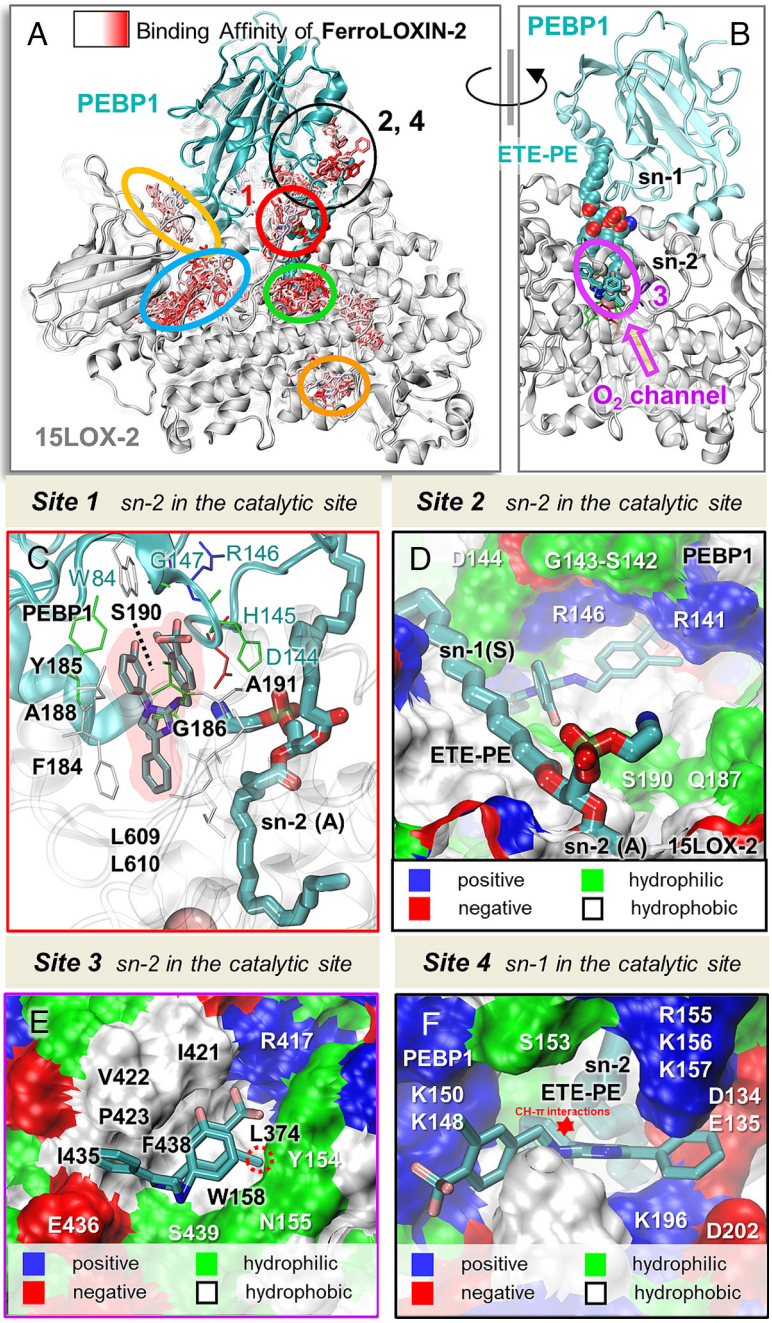

Fig. 3. Binding sites and poses of new compounds on the 15LOX-2/PEBP1/ETE-PE complex, illustrated for FerroLOXIN-2. (*A* and *B*) Most frequent binding poses of FerroLOXIN-2 are shown [in *sticks*, colored from *white* (low affinity) to *red* (high affinity)] upon superposition of the results from multiple docking simulations. The ellipses indicate probable binding sites. Those labeled *Sites 1, 2* and *4* in *A*, *Site 3* viewed from back in (*B*) are high affinity sites specific to 15LOX-2/PEBP1, and *Site 1* is exclusively accessed in the presence of ETE-PE. *Site 3* involves gating residues Y154 and W158 at the entrance of an O_2 channel in 15LOX-2. (*C–F*) Closeup views of the interactions of the inhibitor (*thin sticks, CPK colors*) with ETE-PE (*thick sticks, CPK*) and with PEBP1 and 15LOX-2 residues (labeled), at the four sites. In panels *D–F*, 15LOX-2/PEBP1 regions lining the binding pocket are colored by hydrophobicity and/or charge, as indicated. In *Site 4*, the compound inhibits 15LOX-2 by displacing the reactive *sn-2* (arachidonic) tail of ETE-PE from the catalytic pocket. See more details in *SI Appendix*, Figs. S7–S9.

respectively (*SI Appendix*, Table S4 and Fig. S11 *A* and *B*). The analysis also revealed that FerroLOXINs possessed much higher plasma and intestine exposure levels as indicated by the higher C_{max} and AUC_{last} levels in both tissues. Notably, the exposure was much higher in the intestine compared to plasma. Overall, the PK profile correlated well with our observed efficacy in the TBI model (Fig. 4 *A* and *B* and *SI Appendix*, Table S4 and Fig. S12).

To examine the radiomitigative effectiveness of FerroLOXINs in vivo, we employed a C57BL/6 mouse model of TBI in which our previous studies demonstrated the accumulation of 15-HpETE-PE suggesting a role of ferroptosis in the disease progression (12). We performed two series of experiments with female and male mice, respectively. Typical of the female model, irradiation to a dose of 9.25Gy caused 100% lethality on day 19 after irradiation (Fig. 4*A*). Both FerroLOXIN-1 and 2 (at a dose of 25 mg/kg, ip-injected 24 h after radiation) exerted robust radiomitigative effects. The survival on day 19 was estimated at 75 and 80%, respectively (Fig. 4*A*). Confocal microscopy revealed significant damage to the intestinal epithelium on day 5 after TBI. The breach of epithelial lining—assessed by the disintegration of the actin layer (*green*) (Fig. 4*B*)—was clearly observed in irradiated mice. The ileum damage was significantly mitigated in mice treated

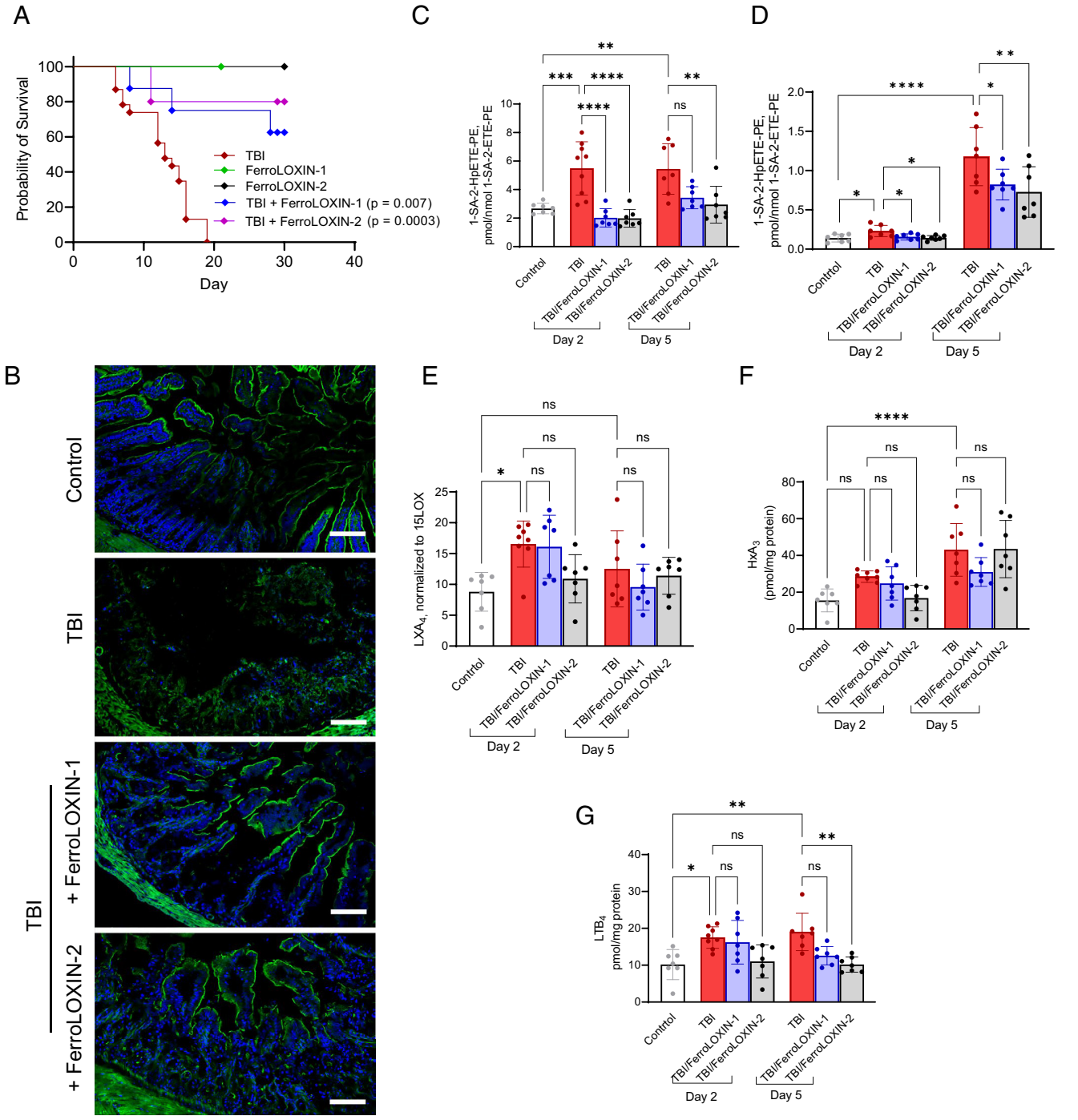

Fig. 4. FerroLOXIN-1 and FerroLOXIN-2 rescue mice from TBI induced death by inhibiting ferroptosis (*A*) FerroLOXIN-1 and FerroLOXIN-2 alters the survival of irradiated mice. 24 h after TBI, C57BL/6NTac mice were left alone (TBI) or treated with either FerroLOXIN-1 or FerroLOXIN-2 (25 mg/kg) and monitored for 30 d. (*B*) Treatment with FerroLOXINs mitigated TBI induced epithelial disintegration assessed by discontinuity of actin layer (green). (Scale 40 μm.) (*C*) FerroLOXINs mitigate accumulation of proferroptotic signal HpETE-PE in ileum (*C*) and bone marrow (*D*) of irradiated mice. Levels of lipoxin A4 (*E*) and leukotriene B4 (*F*) and hepoxilin A3 (*G*) in mouse ileum. Ileum samples were collected on days 2 and 5 after TBI and processed for redox-lipidomics. Data represents mean ± SD, n = 7 mice/group; $*P < 0.05$, $**P < 0.01$, $***P < 0.001$, $****P < 0.0001$, One-way ANOVA, Tukey's multiple comparison test.

with either FerroLOXIN-1 or 2 (Fig. 4*B*). We also performed TBI experiments using male mice. As males are more sensitive to irradiation than females (34), we used a lower dose of 9.0 Gy TBI. This dose caused 100% lethality on day 15 after irradiation (*SI Appendix*, Fig. S12). Similar to females, FerroLOXIN-1 and 2 (at 25 mg/kg, ip-injected 24 h after radiation) exerted a significant albeit less potent radiomitigative effect in male mice (*SI Appendix*, Fig. S12). FerroLOXIN-1 and 2 had no toxic effects in nonirradiated female and male mice (Fig. 4*A* and *SI Appendix*, Fig. S12).

We further used redox lipidomics to determine the effects of FerroLOXINs on the levels of proferroptotic PEox in the ileum and bone marrow of irradiated animals. We detected significantly increased levels of HpETE-PE on days 2 and 5 after irradiation of female mice (Fig. 4*C*). In another radiosensitive tissue, bone marrow (35, 36), LC-MS measurements also revealed significantly increased levels of HpETE-PE on days 2 and 5 after TBI (Fig. 4*D*), whereby, the contents of HpETE-PE were higher on day 5 vs. day 2. To confirm the structure of HpETE-PE detected in the ileum and bone

marrow, we performed MS^2 analysis (*SI Appendix*, Fig. S13 *A* and *B*). Characteristic MS^2 fragments attributed to the polar head of PE with m/z 140.009 and 196.036 were detected. The fragments [R_1-H]-, [R_2-H]-, [R_2-H_2O-H]-, and [M-H-R_2CH=C=O]- present in the MS^2 spectra correspond to: i) stearic acid in *sn*-1 position, ii) HpETE in *sn*-2 position, iii) dehydrated HpETE, and iv) an ion generated with loss of *sn*-2 HpETE as ketene (*SI Appendix*, Fig. S13*B*). Most importantly, both FerroLOXINs significantly mitigated the TBI-induced generation of proferroptotic death signal in the ileum and bone marrow of irradiated mice on days 2 and 5 after TBI (Fig. 4 *C* and *D*).

TBI-induced inflammatory disease is a multistep process involving multiple mechanisms and culminating in several types of cell death programs (37). To determine the extent to which mitigative effects of FerroLOXIN-1 and 2 might be associated with inhibition of TBI-induced ferroptosis vs. other cell death pathways, we performed redox lipidomic analysis focused on oxygenated phospholipids acting as signals of apoptosis and necroptosis, hydroxycardiolipin, CL-(72:7-OH) and hydroperoxy-phosphatidylcholine, PC-(40:8-OOH), respectively (38, 39). While a significantly elevated level of CL-(72:7-OH) was detected in the ileum on day 2 after irradiation, its content was not changed after treatment with either FerroLOXIN-1 or 2 (*SI Appendix*, Fig. S14*A*). This suggests that radiomitigative effects of FerroLOXINs were not associated with apoptosis. LC/MS assessment of necroptotic PC-(40:8-OOH) signals revealed no significant differences on days 2 and 5 after TBI and their contents were not affected by FerroLOXINs (*SI Appendix*, Fig. S14*B*). Thus, the radiomitigative effects of FerroLOXINs cannot be attributed to the inhibition of either apoptotic or necroptotic cell deaths.

We further explored whether FerroLOXINs affected the contents of lipid mediators generated by 15LOX (33, 40). On day 2 after irradiation, LC-MS analysis showed significantly elevated levels of an anti-inflammatory mediator, lipoxin A_4 (LXA_4) generated from AA by 15LOX (33, 40, 41) (Fig. 4*E*). This TBI-induced signal was not significantly affected by either of the tested FerroLOXINs (Fig. 4*E*). Redox lipidomics also revealed a significant accumulation of proinflammatory mediator, hepoxilin A_3 (HXA_3), generated by 12LOX (42), on day 5 after TBI (Fig. 4*F*). FerroLOXINs did not change the level of HXA_3 (Fig. 4*F*). Interestingly, elevated levels of leukotriene B_4 (LTB_4) were detected on day 2 and 5 after TBI (Fig. 4*G*). The content of LTB_4 was significantly lower on day 5 only in the presence of FerroLOXIN-2**.** Given that LTB_4 is synthesized by 5LOX in polymorphonuclear neutrophils (PMNs) and macrophages (43), changes in the LTB_4 levels in irradiated intestine may be related to TBI-induced infiltration/clearance of PMNs and macrophages from the affected intestinal sites.

Conclusion

Ferroptosis is a lipid peroxidation-driven cell death, resulting from the selective peroxidation of PUFA-PE to hydroperoxy-PEs (16). To date, a number of ferroptosis inhibitors have been proposed; however, most of them are nonspecific and fall into three major categories; i) radical trapping agents (TRAs), like ferrostatin 1, liproxstatin 1, and α-tocopherol; ii) iron chelators, like DFO, and iii) pan-LOX inhibitors, like baicalein and zileuton (44). In the enzymatically controlled generation of proferroptotic signals, the specificity of 15LOX-2 is endowed by its association with a scaffolding protein, PEBP1 (1, 11). The role of 15LOX-2/PEBP1 in generating the peroxidized ETE-PE molecules, which serve as proferroptotic signals, is now well-established (11, 19, 29).

While the functions of the majority of other peroxidized lipids are still largely enigmatic, several have been associated with immunosuppressive functions in tumor microenvironment (45, 46), antigen cross-presentation by dendritic cells (47), re-awakening of dormant tumor cells (48), execution of other programs of regulated cell death as an alternative to ferroptosis (e.g., apoptosis, necroptosis and pyroptosis) (49), cell proliferation (6), and regulation of pro- and anti-inflammatory responses (46, 49). The nonspecific indiscriminative blockade of all these functions could lead to poorly predictable side effects. One such nonselective mechanism is radical scavenging (50). Indeed, LOXs, like other oxygenases rely on the abstraction of bis-allylic hydrogen and sequential formation of carbon-centered and peroxyl radicals of the oxidizable PUFA substrates (51, 52). While the specificity of these reactions is commonly restricted by protein structural features, promiscuous small molecule radical traps may get access to the reactive radical intermediates, hence interfering with the oxidation process in nonspecific ways (44). With these features in mind, our design of anti-ferroptotic agents was based on the presumption of their poor radical scavenging and iron chelation activity. Indeed, a direct assessment of both of these nonspecific activities of FerroLOXINs using the DPPH assay or detection of ascorbyl radicals by EPR showed their negligible radical trapping activity vs. α-tocopherol or iron chelation ability vs. DFO. In line with this result and our SAR studies, the two lead compounds demonstrated specificity toward the 15LOX-2/PEBP1 complex and not to 15LOX-2 alone. We also demonstrated the specificity of these compounds as inhibitors of ferroptosis and incompetence against other cell death programs. Further, our results suggest that FerroLOXINs have no significant influence on lipid mediators derived from gut epithelium like LXA4 and HXA3 (40, 41). While the literature indicates the range of doses causing predominantly hematopoietic syndrome as 0.7 to 10 Gy and doses >10 Gy are associated predominantly with GI syndrome, symptoms of GI syndrome have been reported even at 6 Gy (53). The radiation responses are strongly dependent on the mouse strains used, age and sex, nutritional factors, the gut microbiota and metabolites, time at which the mice were irradiated and many other factors (54–57). Importantly, we found that FerroLOXINs protect the epithelial breach triggered by radiation as well as mitigate the ferroptotic death both in ileum and bone marrow.

To further understand the mechanisms of the antiferroptotic action of the new compounds on the 15LOX-2/PEBP1 complex, we carried out extensive modeling and simulations of the interactions of the selected compounds with 15LOX-2 and the 15LOX-2/PEBP1 complex. Simulations revealed three potential mechanisms of inhibition (Fig. 3). *Mechanism 1* has the inhibitors binding at *Site 1* or *Site 2*, localized between PEBP1 and 15LOX-2, which alters the position of the buried oxidizable *sn-2* chain so that it moves either partially or completely out of the catalytic site (*SI Appendix*, Fig. S9*A* and Movie S1), thereby preventing the enzymatic reaction. These interactions also weaken the 15LOX-2/PEBP1 interface, thus destabilizing the cooperative motions gained upon complexation (11, 19). *Mechanism 2* is via inhibitor binding at *Site 3* and blocking the predominant oxygen channel (28, 29) to 15LOX-2 catalytic pocket (Fig. 3*E*, *SI Appendix*, Fig. S8, and Movies S2 and S3). Therefore, this mechanism effectively obstructs the oxidation process. Considering that the substrate ETE-PE can temporarily bind to 15LOX-2 catalytic site through its nonoxidizable *sn-1* chain, we investigated the possible occurrence of *Mechanism 3*, i.e., binding of the compounds to the 15LOX-2/PEBP1/ETE-PE interface to prevent the nonoxidizable chain from leaving the catalytic site thereby hampering the catalytic activity. Extended simulations demonstrated that in the presence of inhibitors the substrate

remained bound in this nonoxidizable conformation for up to 0.55 microseconds. *Mechanism 3* was valid for all inhibitors, in contrast to the other two mechanisms which were inhibitor-specific.

Overall, our results demonstrate the possibility of inhibiting ferroptosis by designing highly selective inhibitors of the 15LOX-2/PEBP1 catalytic complex. The latter is essential for initiating ferroptotic cell death in a number of disease conditions, such as acute radiation syndrome, brain trauma, kidney damage (11), and cardiovascular and neurodegenerative diseases (58, 59). These inhibitors and this approach may be useful for the development of new therapeutics for specific suppression of 15LOX/PEBP1 complexes important to a plethora of serious human diseases.

Materials and Methods

Design and Synthesis of Chemical Compounds. All the methods and protocols used for the synthesis of compounds and their detailed characterization are described in *SI Appendix*, *Supplementary Methods*.

Reagents. Phospholipids were purchased from Avanti Polar Lipids or Cayman Chemicals (See *SI Appendix* for details). All other reagents used in this study are described in *SI Appendix*, *Supplementary Methods*.

Mice. C57BL/6NTac female or male mice (7 to 8 wk) were from Taconic Biosciences (Germantown, NY) and were housed under specific pathogen-free conditions at the Hillman Animal Research Facility, University of Pittsburgh, Pittsburgh, PA. All protocols were approved by the Institutional Animal Care and Use Committee of the University of Pittsburgh (IACUC number 21028741). Veterinary care was provided by the Division of Laboratory Animal Resources of the University of Pittsburgh.

Cell Death Assays. Ferroptosis in human bronchial epithelial cells- HBE, cancer cells–HT-1080 and A375, and intestinal epithelial cells–Caco2 and FHs 74 Int, was induced by RSL3 and assessed by flow cytometry using propidium iodide (PI) staining as described previously (32). HBE cells were also used for studying necroptosis (TNF-α, SM-164 and zVAD.fmk), pyroptosis (LPS and Nigericin) and apoptosis (Staurosporine) in presence of FerroLOXINs. Details are provided in *SI Appendix, Supplementary Methods*.

Iron Chelation Activity. EPR spectroscopy was used to assess the iron chelation activity of FerroLOXIN-1 and 2. Briefly, magnitudes of the EPR signals of semidehydroascorbyl radicals formed during the reduction of Fe(III) with ascorbic acid were recorded in the absence or presence of FerroLOXINs or deferoxamine (DFO). See *SI Appendix*, *Supplementary Methods*.

Confocal Microscopy. Mouse ileum sections (5 μm.) were washed in PBS and incubated in Alexa Fluor 647 phalloidin (Invitrogen, A22287) for 45 min. Nuclei were stained with Hoechst (Sigma, B2883) 1 mg/100 mL dH20 for one minute, washed in PBS, and mounted in gelvatol. Large area scan images were obtained on Nikon A1 confocal microscope with NIS Elements v5.39.02.4 at 40× magnification.

Molecular Simulations. We performed both socking and full-atomic MD simulations. Docking simulations are described in the *SI Appendix, Supplementary Methods*. MD simulations of 200 to 550 ns were performed for systems selected from molecular docking (*SI Appendix*, Table S2) using the NAMD software with the CHARMM force field, and 2 fs time steps. The proteins were solvated with explicit water models (TIP3P). See *SI Appendix, Supplementary Methods* for details on this and all methods described below.

TBI. C57BL/6NTac (female or male) were irradiated (9.25 Gy or 9.0 Gy, respectively) using a Model 68a cesium irradiator (JL Shephard and Associates, San Fernando, CA) and then 24 h after radiation exposure FerroLOXIN-1 or FerroLOXIN-2 (25 mg/kg body weight in single-drug regimen) were injected intraperitoneally (12).

Isolation and Cells Dissociation of Mouse Ileum and Flow Cytometry Analysis. Samples of ileum from control, irradiated, irradiated + FerroLOXIN-1 and 2 C57BL/6 mice were isolated, rinsed in cold PBS, opened longitudinally, and sliced into the small fragments and processed for cell dissociation and analyses described in the *SI Appendix*.

Oxidation of *sn-1*-Stearoyl-*sn-2*-Arachidonoyl-Phosphatidylethanolamine (1-SA-2-AA-PE) by 15-Lipoxygenase-2 (LOX15-2) in a Model System. Activity of 15LOX-2 was assessed by formation of primary products of 15-HpETE-PE. Briefly, SAPE:DOPC liposomes (see *SI Appendix* for liposome preparation) were incubated with human recombinant 15LOX-2 (0.4 μM) or 15LOX-2/PEBP1 complex (1:1 ratio) (see *SI Appendix* for 15-LOX2 and PEBP1 protein purification) in the presence or absence of inhibitors (0.25 μM) for 20 min at 37 °C. The inhibitors were added before the addition of enzyme to the reaction mixture containing 13-hydroperoxy-octadecadienoic acid (13(S)-HpODE) (3 μM) for activation of 15LOX-2.

Structure and PKs of FerroLOXIN-1 and 2. Structures of FerroLOXINs were confirmed by MS^2 analysis using Fusion Lumos Tribrid mass spectrometer (Thermo Scientific, USA). In vivo PK analysis was performed at ChemoGenics BioPharma. Details can be found in the *SI Appendix*, Supplementary Methods.

Redox Phospholipidomics. LC/ESI-MS analyses of lipids, oxygenated lipids (including proferroptotic signals) were performed on a Thermo HPLC system coupled to either an Orbitrap Fusion Lumos mass spectrometer (ThermoFisher Scientific) for normal phase analysis or a Q-Exactive mass spectrometer (ThermoFisher Scientific) for reverse-phase (C30) analysis.

Statistical Analysis. Statistical analyses were performed with GraphPad Prism 9.2.0 (GraphPad Software Inc.) by one-way ANOVA, Tukey's multiple comparisons test, unless otherwise specified.

Data, Materials, and Software Availability. Data and codes generated during the study and included in this article are available from the corresponding authors upon request. Requests for the inhibitors should be directed to corresponding authors and National Center for Advancing Translational Science (NCATS).

ACKNOWLEDGMENTS. This work was supported by NIH (HL114453, U01AI156924, U01AI156923, CA165065, NS076511, NS061817, P41GM103712, P01DK096990 and R01GM139297), by Polish National Science Centre no. 2019/35/D/ST4/02203. K.M.-R. is thankful for the facilities and computer time allocated by the Interdisciplinary Center for Modern Technologies (Nicolaus Copernicus University) for quantum chemistry calculations in Gaussian. D.K.L., A.Y., A.V.Z., S.R.; A.B.S, J.M., and G.R. acknowledge the funding from the Intramural Research Program, National Center for Advancing Translational Sciences, NIH. We thank Sam Michael for automation support; Paul Shinn, Misha Itkin, Zina Itkin, Glen Gomba, and Danielle van Leer for the assistance with compound management; Christopher LeClair, Paul Will, and Kamaria Butler for analytical chemistry and compound purification support.

Author affiliations: [a]Department of Environmental and Occupational Health, Center for Free Radical and Antioxidant Health, University of Pittsburgh, Pittsburgh, PA 15260; [b]Department of Biophysics, Faculty of Physics Astronomy and Informatics, Institute of Physics, Nicolaus Copernicus University in Toruń, Toruń, Poland; [c]National Center for Advancing Translational Sciences, Rockville, MD 20892; [d]Department of Radiation Oncology, University of Pittsburgh, Pittsburgh, PA 15260; [e]Department of Chemistry and Biochemistry, University of California Santa Cruz, Santa Cruz, CA 95064; [f]Department of Cell Biology, University of Pittsburgh, Pittsburgh, PA 15260; [g]Department of Biological Sciences, University of Pittsburgh, Pittsburgh, PA 15260; [h]Department of Internal Medicine, The Ohio State University, Columbus, OH 43210; [i]Department of Pediatrics, Division of Critical Care and Hospital Medicine, Redox Health Center, Vagelos College of Physicians and Surgeons, Columbia University Irving Medical Center, New York, NY 10032; and [j]Laufer Center for Physical Quantitative Biology and Department of Biochemistry and Cell Biology, School of Medicine, Stony Brook University, NY 11794

Author contributions: H.H.D., Y.Y.T., A.B.S, J.M., R.K.M., S.E.W., J.S.G., G.R., H.B., I.B., and V.E.K. designed research; H.H.D., K.M.-R., D.K.L., A.Y., S.N.S., A.A.K., A.B.S., M.W.E., G.V.S., M.S., C.M.S.C., S.C.W., S.R., and A.V.Z. performed research; T.R.H. and A.P.V. contributed new reagents/analytic tools; H.H.D., K.M.-R., Y.Y.T., D.K.L., A.Y., S.N.S., A.A.K., A.B.S., V.A.T., A.A.A., M.W.E., G.V.S., T.R.H., C.M.S.C., S.C.W., A.P.V., S.R., A.V.Z., A.S., J.M., R.K.M., J.S.G., G.R., H.B., I.B., and V.E.K. analyzed data; and H.H.D., K.M.-R., Y.Y.T., G.R., H.B., I.B., and V.E.K. wrote the paper.

Reviewers: N.V.D., Penn State Milton S. Hershey Medical Center; E.C.L., Georgetown University; G.S., University of Colorado Anschutz Medical Campus; and S.T., Nagoya University Graduate School of Medicine.

Competing interest statement: I.B. and N.V.D. are co-authors on a 2019 review paper and have not collaborated after that.

1. V. E. Kagan *et al.*, Redox epiphospholipidome in programmed cell death signaling: Catalytic mechanisms and regulation. *Front. Endocrinol.* **11**, 628079 (2021).
2. D. Tang, R. Kang, T. V. Berghe, P. Vandenabeele, G. Kroemer, The molecular machinery of regulated cell death. *Cell Res.* **29**, 347–364 (2019).
3. X. Chen, R. Kang, G. Kroemer, D. Tang, Organelle-specific regulation of ferroptosis. *Cell Death Differ.* **28**, 2843–2856 (2021).
4. S. J. Dixon *et al.*, Ferroptosis: An iron-dependent form of nonapoptotic cell death. *Cell* **149**, 1060–1072 (2012).
5. B. R. Stockwell, Ferroptosis turns 10: Emerging mechanisms, physiological functions, and therapeutic applications. *Cell* **185**, 2401–2421 (2022).
6. B. R. Stockwell *et al.*, Ferroptosis: A regulated cell death nexus linking metabolism, redox biology, and disease. *Cell* **171**, 273–285 (2017).
7. X. Jiang, B. R. Stockwell, M. Conrad, Ferroptosis: Mechanisms, biology and role in disease. *Nat. Rev. Mol. Cell Biol.* **22**, 266–282 (2021).
8. L. Yang, L.-M. Cao, X.-J. Zhang, B. Chu, Targeting ferroptosis as a vulnerability in pulmonary diseases. *Cell Death Dis.* **13**, 1–14 (2022).
9. P. Lei, S. Ayton, A. I. Bush, The essential elements of Alzheimer's disease. *J. Biol. Chem.* **296**, 100105 (2021).
10. C. Liang, X. Zhang, M. Yang, X. Dong, Recent progress in ferroptosis inducers for cancer therapy. *Adv. Mater.* **31**, 1904197 (2019).
11. S. E. Wenzel *et al.*, PEBP1 wardens ferroptosis by enabling lipoxygenase generation of lipid death signals. *Cell* **171**, 628–641 (2017).
12. H. H. Dar *et al.*, *P. aeruginosa* augments irradiation injury via 15-lipoxygenase-catalyzed generation of 15-HpETE-PE and induction of theft-ferroptosis. *JCI Insight* **7**, e156013 (2022).
13. W. Li *et al.*, Necroptosis triggers spatially restricted neutrophil-mediated vascular damage during lung ischemia reperfusion injury. *Proc. Natl. Acad. Sci. U.S.A.* **119**, e2111537119 (2022).
14. H. Bayır *et al.*, Achieving life through death: Redox biology of lipid peroxidation in ferroptosis. *Cell Chem. Biol.* **27**, 387–408 (2020).
15. S. Doll, M. Conrad, Iron and ferroptosis: A still ill-defined liaison. *IUBMB life* **69**, 423–434 (2017).
16. V. E. Kagan *et al.*, Oxidized arachidonic and adrenic PEs navigate cells to ferroptosis. *Nat. Chem. Biol.* **13**, 81–90 (2017).
17. M. Conlon *et al.*, A compendium of kinetic modulatory profiles identifies ferroptosis regulators. *Nat. Chem. Biol.* **17**, 665–674 (2021).
18. A. Seiler *et al.*, Glutathione peroxidase 4 senses and translates oxidative stress into 12/15-lipoxygenase dependent-and AIF-mediated cell death. *Cell Metab.* **8**, 237–248 (2008).
19. T. S. Anthonymuthu *et al.*, Empowerment of 15-lipoxygenase catalytic competence in selective oxidation of membrane eTE-PE to ferroptotic death signals, HpETE-PE. *J. Am. Chem. Soc.* **140**, 17835–17839 (2018).
20. N. H. Schebb *et al.*, Formation, signaling and occurrence of specialized pro-resolving lipid mediators–What is the evidence so far? *Front. Pharmacol.* **13**, 838782 (2022).
21. R. Mashima, T. Okuyama, The role of lipoxygenases in pathophysiology; new insights and future perspectives. *Redox Biol.* **6**, 297–310 (2015).
22. R. G. Snodgrass, B. Brüne, Regulation and functions of 15-lipoxygenases in human macrophages. *Front. Pharmacol.* **10**, 719 (2019).
23. K. Mikulska-Ruminska *et al.*, Characterization of differential dynamics, specificity, and allostery of lipoxygenase family members. *J. Chem. Inf. Model.* **59**, 2496–2508 (2019).
24. J. B. Jameson *et al.*, A high throughput screen identifies potent and selective inhibitors to human epithelial 15-lipoxygenase-2. *PLoS One* **9**, e104094 (2014).
25. W.-C. Tsai *et al.*, Kinetic and structural investigations of novel inhibitors of human epithelial 15-lipoxygenase-2. *Bioorg. Med. Chem.* **46**, 116349 (2021).
26. V. E. Kagan, N. V. Gorbunov, EPR measurements of nitric oxide-induced chromanoxyl radicals of vitamin E. Interactions with vitamin C. *Methods Mol. Biol.* **108**, 277–284 (1998).
27. A. Baschieri, R. Amorati, Methods to determine chain-breaking antioxidant activity of nanomaterials beyond DPPH•. A review. *Antioxidants* **10**, 1551 (2021).
28. S. Zhang *et al.*, ProDy 2.0: Increased scale and scope after 10 years of protein dynamics modelling with python. *Bioinformatics* **37**, 3657–3659 (2021).
29. A. A. Kapralov *et al.*, Redox lipid reprogramming commands susceptibility of macrophages and microglia to ferroptotic death. *Nat. Chem. Biol.* **16**, 278–290 (2020).
30. K. Mikulska-Ruminska *et al.*, NO• represses the oxygenation of arachidonoyl PE by 15LOX/PEBP1: Mechanism and role in ferroptosis. *Inter. J. Mol. Sci.* **22**, 5253 (2021).
31. T. S. Anthonymuthu *et al.*, Resolving the paradox of ferroptotic cell death: Ferrostatin-1 binds to 15LOX/PEBP1 complex, suppresses generation of peroxidized ETE-PE, and protects against ferroptosis. *Redox Biol.* **38**, 101744 (2020).
32. H. H. Dar *et al.*, Pseudomonas aeruginosa utilizes host polyunsaturated phosphatidylethanolamines to trigger theft-ferroptosis in bronchial epithelium. *J. Clin. Invest.* **128**, 4639–4653 (2018).
33. N. K. Singh, G. N. Rao, Emerging role of 12/15-Lipoxygenase (ALOX15) in human pathologies. *Prog. Lipid Res.* **73**, 28–45 (2019).
34. N. Narendran, L. Luzhna, O. Kovalchuk, Sex difference of radiation response in occupational and accidental exposure. *Front. Genet.* **10**, 260 (2019).
35. S. Garg *et al.*, Influence of sublethal total-body irradiation on immune cell populations in the intestinal mucosa. *Radiat. Res.* **173**, 469–478 (2010).
36. J. P. Williams, W. H. McBride, After the bomb drops: A new look at radiation-induced multiple organ dysfunction syndrome (MODS). *Int. J. Radiat. Biol.* **87**, 851–868 (2011).
37. J. Steinman *et al.*, Improved total-body irradiation survival by delivery of two radiation mitigators that target distinct cell death pathways. *Radiat. Res.* **189**, 68–83 (2018).
38. G. Mao *et al.*, Mitochondrial redox opto-lipidomics reveals mono-oxygenated cardiolipins as pro-apoptotic death signals. *ACS Chem. Biol.* **11**, 530–540 (2016).
39. B. Wiernicki *et al.*, Excessive phospholipid peroxidation distinguishes ferroptosis from other cell death modes including pyroptosis. *Cell Death Dis.* **11**, 922 (2020).
40. S. Tornhamre, A. Elmqvist, J. A. Lindgren, 15-Lipoxygenation of leukotriene A(4). Studies Of 12- and 15-lipoxygenase efficiency to catalyze lipoxin formation. *Biochim. Biophys. Acta* **1484**, 298–306 (2000).
41. W. W. Christie, J. L. Harwood, Oxidation of polyunsaturated fatty acids to produce lipid mediators. *Essays Biochem.* **64**, 401–421 (2020).
42. S. Nigam *et al.*, The rat leukocyte-type 12-lipoxygenase exhibits an intrinsic hepoxilin A3 synthase activity. *J. Biol. Chem.* **279**, 29023–29030 (2004).
43. O. Rådmark, O. Werz, D. Steinhilber, B. B. Samuelsson, 5-Lipoxygenase, a key enzyme for leukotriene biosynthesis in health and disease. *Biochim. Biophys. Acta* **1851**, 331–339 (2015).
44. J. P. F. Angeli, R. Shah, D. A. Pratt, M. Conrad, Ferroptosis inhibition: Mechanisms and opportunities. *Trends Pharmacol. Sci.* **38**, 489–498 (2017).
45. L. Jiang *et al.*, Ferroptosis as a p53-mediated activity during tumour suppression. *Nature* **520**, 57–62 (2015).
46. C. Mao *et al.*, DHODH-mediated ferroptosis defence is a targetable vulnerability in cancer. *Nature* **593**, 586–590 (2021).
47. B. Wiernicki *et al.*, Cancer cells dying from ferroptosis impede dendritic cell-mediated anti-tumor immunity. *Nat. Commun.* **13**, 3676 (2022).
48. Y. Mou *et al.*, Ferroptosis, a new form of cell death: Opportunities and challenges in cancer. *J. Hematol. Oncol.* **12**, 34 (2019).
49. R. Demuynck, I. Efimova, F. Naessens, D. V. Krysko, Immunogenic ferroptosis and where to find it? *J. Immunother. Cancer* **9**, e003430 (2021).
50. M. E. Alberto, N. Russo, A. Grand, A. Galano, A physicochemical examination of the free radical scavenging activity of Trolox: Mechanism, kinetics and influence of the environment. *Phys. Chem. Chem. Phys.* **15**, 4642–4650 (2013).
51. A. Andreou, I. Feussner, Lipoxygenases–Structure and reaction mechanism. *Phytochemistry* **70**, 1504–1510 (2009).
52. R. Suardíaz *et al.*, Understanding the mechanism of the hydrogen abstraction from arachidonic acid catalyzed by the human enzyme 15-lipoxygenase-2. A quantum mechanics/molecular mechanics free energy simulation. *J. Chem. Theory Comput.* **12**, 2079–2090 (2016).
53. J. Wang *et al.*, Total body irradiation in the "Hematopoietic" dose range induces substantial intestinal injury in non-human primates. *Radiat. Res.* **184**, 545–553 (2015).
54. W. R. Hanson *et al.*, Comparison of intestine and bone marrow radiosensitivity of the BALB/c and the C57BL/6 mouse strains and their B6CF1 offspring. *Radiat. Res.* **110**, 340–352 (1987).
55. J. K. Waselenko *et al.*, Medical management of the acute radiation syndrome: Recommendations of the strategic national stockpile radiation working group. *Ann. Intern. Med.* **140**, 1037–1051 (2004).
56. C. Booth, G. Tudor, J. Tudor, B. P. Katz, T. J. MacVittie, Acute gastrointestinal syndrome in high-dose irradiated mice. *Health Phys.* **103**, 383–399 (2012).
57. H. Guo *et al.*, Multi-omics analyses of radiation survivors identify radioprotective microbes and metabolites. *Science* **370**, eaay9097 (2020).
58. W.-Y. Sun *et al.*, Phospholipase iPLA 2 β averts ferroptosis by eliminating a redox lipid death signal. *Nat. Chem. Biol.* **17**, 465–476 (2021).
59. C. O. Reichert *et al.*, Ferroptosis mechanisms involved in neurodegenerative diseases. *Int. J. Mol. Sci.* **21**, 8765 (2020).